International Journal of Automotive Technology, Vol. 19, No. 4, pp. 669−676 (2018)
DOI 10.1007/s12239−018−0064−6

Copyright © 2018 KSAE/ 103−10
pISSN 1229−9138/ eISSN 1976−3832

TIRE LATERAL FORCE ESTIMATION USING KALMAN FILTER

Eunjae Lee[1)], Hojin Jung[2)] and Seibum Choi[2)*]

[1)]Hankook Tire R&D Center, 50, Yuseong-daero 935beon-gil, Yuseong-gu, Daejeon 34127, Korea
[2)]Mechanical Engineering Department, KAIST, Daejeon 34141, Korea

(Received 26 July 2017; Revised 28 November 2017; Accepted 4 December 2017)

ABSTRACT−As for the tire analysis, lateral tire force is a fundamental factor that describes the stability of vehicle handling. Attempts to analyze the vehicle stability have been made based on various objective test methods and some specific factors such as yaw, lateral acceleration and roll angle. However, the problem to identify which axle is lack of the tire grip at a certain situation still remains. Since indoor tire force measurement system cannot represent a real road and vehicle conditions, tire force measurement through a real vehicle test is inevitable. Due to the high price of the tire force measurement device, tire force estimator can be an alternative toward cost reduction and device failure. In this paper, nonlinear planar full car model combined with tire model is proposed. Then, using discrete-time extended Kalman-Bucy filter (EKBF), individual tire lateral force are estimated with modified relaxation length model.

KEY WORDS : Kalman filter, Relaxation length, Tire force estimation, Planar full car model, Cornering stiffness model

NOMENCLATURE

V_x	: longitudinal velocity, m/s
V_y	: lateral velocity, m/s
γ	: yaw rate, rad/s
m	: vehicle mass, kg
I_z	: moment of inertia about yaw axis, kg m^2
δ_1	: left wheel steer angle, rad
δ_2	: right wheel steer angle, rad
t	: half of vehicle track width, m
l_f	: distance from front axle to the center of gravity, m
l_r	: distance from rear axle to the center of gravity, m
ρ_{air}	: density of air, kg/m^3
C_d	: drag coefficient, -
A	: vehicle front cross sectional area, m^2
ϕ	: roll angle, rad
ε_f	: front roll steer compliance, -
ε_r	: rear roll steer compliance, -
l	: wheel base length, m
h_{cg}	: height from ground to center of gravity, m
$c_{\varphi f}$	: front roll stiffness, nm/rad
$c_{\varphi r}$	: rear roll stiffness, nm/rad
h_r	: distance from cg to roll axis, m
R_r	: rolling resistance, -
R_e	: effective radius, m
μ	: road friction coefficient, -
σ	: relaxation length, m
C_α	: cornering stiffness, N/rad
K_L	: lateral stiffness, N/m
K_D	: distortion stiffness, Nm/rad

*Corresponding author. e-mail: sbchoi@kaist.ac.kr

SUBSCRIPT

fl, *fr*, *rl*, *rr* : front left, front right, rear left, rear right

1. INTRODUCTION

Evaluating the steering response and stability of the vehicle have relied on a well-trained evaluator called subjective test engineer. This have been known to be the most reliable test method that cannot be replaced in the industry. To analyse the subjective test results physically, pseudo objective test methods and representative parameters were demanded, thereafter a huge variety of indices have been suggested.

Among them, tire force is one of the fundamental factors that describes the stability of handling performance. For deliberate performance evaluation of developed tire product, the indoor tire force measurement system is widely used. The system measures the force versus slip angle directly for various vertical loading conditions. Although it substitutes the tire and road interface characteristics indirectly, it cannot represent a real paved road and vehicle conditions. Then, tire force measurement data of vehicle driving experiment conducted by equipping with wheel force transducer (WFT) sensor has been acquired additionally. However, it is impractical due to the high cost of measurements device. Therefore, the design of tire force estimator is highly required to reduce the cost.

Three common parameters that have been widely used by numerous tire-manufacturing companies for indoor tests are cornering stiffness, lateral stiffness, and distortion stiffness. These three tire parameters comprise the standard

indices to determine the lateral motion of a tire by providing specific physical meanings of the tire lateral motion (Pacejka, 2005; Schilippe, 1954). Then, these parameters can be implemented in a tire relaxation length model. However, conventional model which has been adopted for the lateral dynamics representation includes only cornering stiffness and lateral stiffness. In the aspects of lateral tire force estimation, use of advanced tire relaxation length model can help improve the accuracy of tire lateral force estimation especially in transient response (Higuchi and Pacejka, 1997; Maas, 2009).

To deal with the aforementioned issue, this paper proposes the tire force estimation algorithm designed with extended Kalman-Bucy filter (EKBF) based on nonlinear vehicle dynamic and tire model by off-line processing. Compared with previous studies (Baffet *et al*., 2007; Doumiati *et al*., 2011; Kim, 2009; Ray, 1997), this paper suggests the improved method of lateral tire force estimation by applying modified relaxation length and modified cornering stiffness in the dynamic tire model. Based on the planar full car model, eleven degree of freedom dynamic equations containing lateral and wheel dynamics were used for the estimator design.

The proposed estimator was validated through the comparison of real lateral tire force at each wheel measured from WFT sensor equipped in test vehicle. In the test vehicle, a steering robot and dynamic motion sensors were also equipped for precise reference input and analysis. The validation test mode is double lane change that represents highly transient maneuvers.

The remainder of this paper is organized as follows. In the following section, the vehicle model which will be adopted for the estimator design is introduced. The third section describes the tire model to represent tire-road interaction. In this section, modified relaxation model including distortion stiffness is suggested, which helps to improve the accuracy of the lateral tire dynamic model. The fourth section describes the tire force estimation strategy. And finally the estimation results and the real force value measured by the vehicle tests will be compared in the fifth section.

2. PLANAR FULL CAR MODEL

This study chose three degree of freedom model of vehicle motion states to estimate and verify lateral tire force at all positions. This model has been widely used to describe the vehicle lateral dynamics (Doumiati *et al*., 2011). Based on the states and parameter nominations described at Figure 1, the equations of motion are described as follows:

$$\dot{V}_x = \frac{1}{m}\{F_{xfl}\cos(\delta_1) + F_{xfr}\cos(\delta_2) - F_{yfl}\sin(\delta_1) - \cdots F_{yfr}\sin(\delta_2) + (F_{xrl} + F_{xrr}) - C_{av}V_x^2\} + V_y\gamma \quad (1)$$

$$\dot{V}_y = \frac{1}{m}\{F_{xfl}\sin(\delta_1) + F_{xfr}\sin(\delta_2) + F_{yfl}\cos(\delta_1) + \cdots F_{yfr}\cos(\delta_2) + F_{yrl} + F_{yrr}\} - V_x\gamma \quad (2)$$

$$\dot{\gamma} = \frac{1}{I_z}\Big[l_f\{F_{xfl}\sin(\delta_1) + F_{xfr}\sin(\delta_2) + F_{yfl}\cos(\delta_1) + \cdots F_{yfr}\cos(\delta_2)\} + t\{F_{xfl}\cos(\delta_1) - F_{xfr}\cos(\delta_2) - F_{yfl}\sin(\delta_1) + \cdots F_{yfr}\sin(\delta_2) + F_{xrl} - F_{xrr}\} - l_r(F_{yrl} + F_{yrr})\Big] \quad (3)$$

where V_x, V_y, γ, m, I_z, δ_1, δ_2, t, l_f, l_r are the longitudinal velocity, lateral velocity, yaw rate, vehicle mass, moment of inertia about yaw axis, left wheel steer angle, right wheel steer angle, half of track width, distance from front axle to the center of gravity (CG), and distance from rear axle to the CG, respectively. F_x, F_y are longitudinal tire force and lateral tire force followed by subscripts *fl*, *fr*, *rl*, *rr* representing front left, front right, rear left, rear right, respectively. C_{av} is the lumped parameter to represent the drag resistance, which is expressed as follows:

$$C_{av} = \frac{1}{2}\rho_{air}C_d A \quad (4)$$

where ρ_{air}, C_d, A are density of air, coefficient of air drag and front cross sectional area, respectively.

Front and rear slip angle at each wheel are represented as follows (Kim, 2009):

$$\alpha_{fi} = -(\delta_j + \varepsilon_f\phi) + \tan^{-1}\left(\frac{V_y + l_f\gamma}{V_x}\right),\ i = l, r;\ j = 1, 2 \quad (5)$$

$$\alpha_{ri} = -\varepsilon_r\phi + \tan^{-1}\left(\frac{V_y - l_r\gamma}{V_x}\right),\ i = l, r \quad (6)$$

where ϕ, ε_f, ε_r are roll angle, front roll steer compliance, and rear roll steer compliance, respectively.

2.1. Vertical Load Calculation

The lateral tire force is affected by load transfer while the vehicle is cornering. The amount of load transfer is determined by the vehicle geometry, stiffness of the

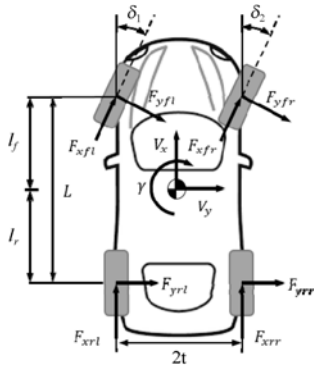

Figure 1. Planar full car model.

suspension, and the spring rate of the tires. In this paper, the linear equation of roll motion and roll stiffness is implemented.

Couplings between the vertical load and lateral force are described as follows (Doumiati *et al*., 2011; Gillespie, 1992; Kim, 2009).

$$\begin{aligned} F_{zfl} &= m_v g\frac{l_r}{2l} - m_v\frac{h_{cg}}{2l}a_x - m_v\frac{h_{cg}l_r}{tl}a_y - \Delta f_{zf} \\ F_{zfr} &= m_v g\frac{l_r}{2l} - m_v\frac{h_{cg}}{2l}a_x + m_v\frac{h_{cg}l_r}{tl}a_y + \Delta f_{zf} \\ F_{zrl} &= m_v g\frac{l_f}{2l} + m_v\frac{h_{cg}}{2l}a_x - m_v\frac{h_{cg}l_f}{tl}a_y - \Delta f_{zr} \\ F_{zrr} &= m_v g\frac{l_f}{2l} + m_v\frac{h_{cg}}{2l}a_x + m_v\frac{h_{cg}l_f}{tl}a_y + \Delta f_{zr} \end{aligned} \tag{7}$$

$$\Delta f_{zi} = \sigma_i m a_y \tag{8}$$

$$\sigma_i = \frac{1}{2t}\left(\frac{c_{\varphi i}}{c_{\varphi f} + c_{\varphi r} - mgh_r}h_r + \frac{l - l_i}{l}h_r\right), i = f, r \tag{9}$$

where l, h_{cg}, a_x, a_y, g, $c_{\varphi f}$, $c_{\varphi r}$, h_r are the wheel base length, height from ground to CG, longitudinal acceleration, lateral acceleration, gravitational acceleration, front roll stiffness, rear roll stiffness, and distance from CG to roll axis, respectively.

2.2. Wheel Dynamics Model

Wheel dynamics can be derived as:

$$\dot{\omega}_i = \frac{1}{I_w}(T_{di} - T_{bi} - R_e F_{xi} - R_e R_r F_{zi}), i = fl, fr, rl, rr \tag{10}$$

where ω_i, I_w, T_{di}, T_{bi}, R_e, F_{xi}, R_r are the wheel angular velocity, wheel moment of inertia, driving torque, braking torque, effective radius, longitudinal force, and rolling resistance coefficient, respectively.

2.3. Output Shaft Torque Dynamics Model

To configure the wheel dynamics equation mentioned above, the information of driving torque transferred from the engine is essential. To consider dynamic model responses such as torque convertor slip and transmission gear shifting event, torque observer can be designed using engine torque and other vehicle data from controller area network (CAN) signal. However, vehicle tests are sometimes conducted without obtaining all vehicle data from CAN signal. For this reason, this paper focuses on the lateral tire force estimation, which allows less accurate drive torque information to be acceptable. Therefore, simplified dynamics model for output shaft torque is applied in this paper. Here output shaft torque is divided into load torque and inertia torque, and inertia torque is expressed by considering drivetrain as a lumped mass as delineated below (Han *et al*., 2016):

$$T_d = J_v\frac{\dot{\omega}_{fl} + \dot{\omega}_{fr}}{2} + T_{L\_model} \tag{11}$$

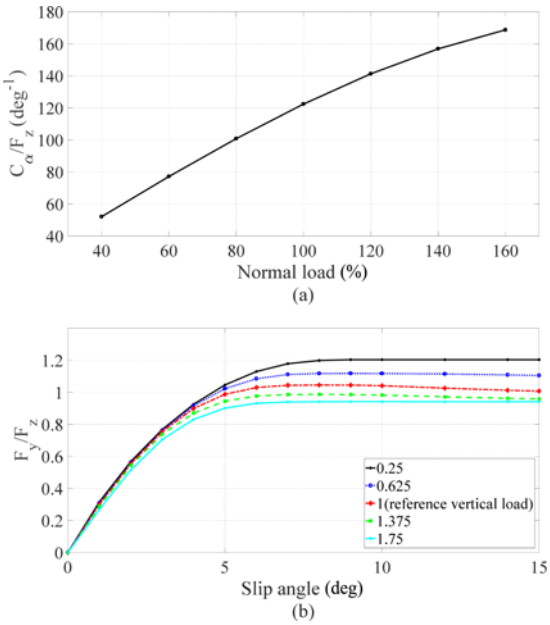

Figure 2. Cornering stiffness variation versus vertical load: (a) Steady cornering; (b) Transient cornering.

$$T_{L\_model} = R_e\left\{R_r F_z + \frac{1}{2}\rho_{air}\left(R_e\frac{\omega_{rl} + \omega_{rr}}{2}\right)^2 C_d A\right\} \tag{12}$$

where T_o and J_v are the output shaft torque and lumped moment of inertia. Here, Equations (11) and (12) apply to front wheel drive type. It is noteworthy that wheel angular velocity is changeable depending on front-wheel-drive or rear-wheel-drive type. The test vehicle used to conduct experiment in this paper was based the on front wheel drive type.

3. TIRE DYNAMICS FOR VEHICLE MODEL INTEGRATION

3.1. Reference Lateral Tire Model

In this paper, Dugoff's model is used as the reference tire model. It expresses the tire force through concerning both of nonlinear characteristics and combined effect of longitudinal and lateral force generation. By neglecting longitudinal force, the simplified nonlinear lateral force is given by (Dugoff *et al*., 1970):

$$\bar{F}_{yi} = -C_{yi}\tan(\alpha_i) f(\lambda_i), i = fl, fr, rl, rr \tag{13}$$

where C_{yi} is the cornering stiffness at each tire position. Here, $f(\lambda_i)$ is expressed as follows:

$$f(\lambda_i) = \begin{cases} (2 - \lambda_i)\lambda_i, & if\ \lambda_i < 1 \\ 1, & if\ \lambda_i \geq 1 \end{cases} \tag{14}$$

$$\lambda_i = \frac{\mu F_z}{2C_{yi}|\tan(\alpha_i)|}, i = fl, fr, rl, rr \tag{15}$$

Here, μ is the road friction coefficient. In this paper, the nominal μ is assumed as 0.9 to represent a nominal high mu surface. With the simplified Dugoff's model, the tire force estimator suggested in this paper focuses on the individual lateral tire force at each wheel.

3.2. Weight Shifting Effect in Cornering Stiffness

Lateral tire force is greatly affected by vertical load changes as well as slip angle during the vehicle maneuvers like double lane change. Therefore, cornering stiffness is also influenced by these effects. Figure 2 shows the experimental result of cornering stiffness variation versus tire vertical load, which is obtained from indoor testing machine of MTS Flat-Trac® test machine. In order to represent the cornering stiffness more precisely in the Dugoff's model, we have reconstructed the cornering stiffness from the simple empirical lateral tire force model that includes both weight shifting and side slip angle term given by:

$$F_{\mathrm{y}} = C_1(F_{\mathrm{z,n}} + k_1\Delta F_z)\alpha + C_2(F_{\mathrm{z,n}} + k_2\Delta F_z)\alpha^2 = C_{\mathrm{y}}\alpha \tag{16}$$

where C_1, C_2 are the cornering stiffness relation coefficients and $F_{\mathrm{z,n}}$, ΔF_{z} are the static vertical load and the difference between dynamic vertical load that includes vehicle acceleration and static vertical load. To improve the accuracy of the lateral force, adjustment factors, k_1 and k_2, are applied to the cornering stiffness equation. These values can be changed according to the test tire characteristics.

From the Equation (16), following modified cornering stiffness C_{y} is adopted in this study:

$$C_{\mathrm{y}} = C_1(F_{\mathrm{z,n}} + k_1\Delta F_z) + C_2(F_{\mathrm{z,n}} + k_2\Delta F_z)\alpha \tag{17}$$

3.3. Dynamic Tire Model

A typical first order dynamic model which expresses the lagged behavior of the lateral tire force can be represented as follows:

$$\frac{\sigma}{V_{\mathrm{x}}}\dot{F}_{\mathrm{yi}} + F_{\mathrm{yi}} = \bar{F}_{\mathrm{yi}},\ i = fl, fr, rl, rr \tag{18}$$

where σ is the relaxation length discussed below.

3.3.1. Modified relaxation length model

Heydinger *et al*. (1991) derived a dynamic model that relates static lateral tire force and lagged lateral tire force. This model expresses the relaxation length as σ, which is represented as follows:

$$\sigma = \frac{C_\alpha}{K_{\mathrm{L}}} \tag{19}$$

where C_α is exactly same as $C_1F_{\mathrm{z,n}}$ and K_{L} is lateral stiffness.

However, according to Lee *et al*. (2016), relaxation length model can be further elaborated through considering three tire characteristic parameters as follows:

$$\therefore \sigma = \left(\frac{C_\alpha^{\,3}}{K_{\mathrm{L}}^{\,3}} - \frac{3C_\alpha K_{\mathrm{D}}}{K_{\mathrm{L}}^{\,2}}\right)^{\frac{1}{3}} \tag{20}$$

where K_{D} is distortion stiffness. This study suggests the improved tire force estimation by applying modified relaxation length model. Experimental result of indoor testing machine is used as nominal values of C_α, K_{L}, K_{D}.

4. ESTIMATOR DESIGN

Based on the literature reviews of the tire forces estimation methods (Baffet *et al*., 2007; Doumiati *et al*., 2011; Kim, 2009; Ray, 1997), Kalman filter has been proved to be more advantageous than other types of estimators, because it takes the stochastic filter form that shows robustness toward parameter uncertainties. Especially, this study adopted extended Kalman-Bucy filter (EKBF) that applies continuous time model in the process of obtaining estimates, because vehicle dynamic response is not that swift compared with measurements of sampling time.

4.1. EKBF Design for States Estimation of Nonlinear Model

By integrating Equations (1) ~ (3), (10) and (18), state space form of the full car vehicle dynamic model is obtained as follows:

$$\dot{\mathbf{x}}(t) = f(\mathbf{x}(t), \mathbf{u}(t)) + \mathbf{w}(t) \tag{21}$$

$$\mathbf{z}(t) = h(\mathbf{x}(t), \mathbf{u}(t)) + \mathbf{v}(t) \tag{22}$$

The state vector, $\mathbf{x}(t)$, is composed of longitudinal velocity, lateral velocity, yaw rate, four wheel angular velocities and tire forces:

$$\mathbf{x}(t) = [V_{\mathrm{x}}, V_{\mathrm{y}}, \gamma, \boldsymbol{\omega}_{[1\times4]}, \mathbf{F}_{[1\times8]}]^{\mathrm{T}} = [x_1, x_2, \cdots, x_{15}]^{\mathrm{T}} \tag{23}$$

Here, the components of the wheel angular velocity and tire force vector are

$$\boldsymbol{\omega}_{[1\times4]} = [\omega_{\mathrm{fl}}, \omega_{\mathrm{fr}}, \omega_{\mathrm{rl}}, \omega_{\mathrm{rr}}] \tag{24}$$

$$\mathbf{F}_{[1\times8]} = [F_{\mathrm{xfl}}, F_{\mathrm{xfr}}, F_{\mathrm{xrl}}, F_{\mathrm{xrr}}, F_{\mathrm{yfl}}, F_{\mathrm{yfr}}, F_{\mathrm{yrl}}, F_{\mathrm{yrr}}] \tag{25}$$

The control input vector is comprised of wheel steer angle and each wheel torque given by:

$$\mathbf{u}(t) = [(\delta_{\mathrm{l}} + \delta_2)/2, T_{\mathrm{di}} - T_{\mathrm{bi}}]^{\mathrm{T}},\ i = fl, fr, rl, rr \tag{26}$$

Here, it was assumed that left and right wheel steer angles are almost same because wheel steer angle is generally obtained from steering wheel angle multiplied by steering gear ratio. Therefore, wheel steer input is expressed as mean value. T_{di} is obtained from the output shaft torque dynamics model explained in Section 2.3.

The measurements are:

$$\mathbf{z}(t) = [V_{\mathrm{x}}, V_{\mathrm{y}}, a_{\mathrm{x}}, a_{\mathrm{y}}, \gamma, \boldsymbol{\omega}_{[1\times4]}]^{\mathrm{T}} \tag{27}$$

Here it is assumed that process noise $\mathbf{w}(t)$ and measurements noise $\mathbf{v}(t)$ are zero mean Gaussian and they are uncorrelated each other.

In Equations (21) and (22), the particular function f and the observation function h are expressed as follows:

$$f = \begin{bmatrix} \frac{1}{m}\{(x_8+x_9)\cos(u_1)-(x_{12}+x_{13})\sin(u_1)+\cdots \\ x_{10}+x_{11}-C_{av}x_1^2\}+x_2x_3 \\ \frac{1}{m}\{(x_8+x_9)\sin(u_1)+(x_{12}+x_{13})\cos(u_1)+\cdots \\ x_{14}+x_{15}\}-x_1x_3 \\ \frac{1}{I_z}\left[l_f\{(x_8+x_9)\sin(u_1)+(x_{12}+x_{13})\cos(u_1)\}+\cdots \right. \\ t\{(x_8-x_9)\cos(u_1)+(-x_{12}+x_{13})\cos(u_1)+\cdots \\ \left. x_{10}-x_{11}\}-l_r(x_{14}+x_{15})\right] \\ \frac{1}{I_w}(u_2-R_ex_8-R_eR_rF_{zfl}) \\ \frac{1}{I_w}(u_3-R_ex_9-R_eR_rF_{zfr}) \\ \frac{1}{I_w}(u_4-R_ex_{10}-R_eR_rF_{zrl}) \\ \frac{1}{I_w}(u_5-R_ex_{11}-R_eR_rF_{zrr}) \\ \mathbf{0}_{[4\times1]} \\ \frac{x_1}{\sigma}(-x_{12}+\bar{F}_{yfl}) \\ \frac{x_1}{\sigma}(-x_{13}+\bar{F}_{yfr}) \\ \frac{x_1}{\sigma}(-x_{14}+\bar{F}_{yrl}) \\ \frac{x_1}{\sigma}(-x_{15}+\bar{F}_{yrr}) \end{bmatrix} \tag{28}$$

$$h = \begin{bmatrix} x_1 \\ x_2 \\ \frac{1}{m}\{(x_8+x_9)\cos(u_1)-(x_{12}+x_{13})\sin(u_1)+\cdots \\ x_{10}+x_{11}-C_{av}x_1^2\} \\ \frac{1}{m}\{(x_8+x_9)\sin(u_1)+(x_{12}+x_{13})\cos(u_1)+\cdots \\ x_{14}+x_{15}\} \\ x_3 \\ x_4 \\ x_5 \\ x_6 \\ x_7 \end{bmatrix} \tag{29}$$

Here, longitudinal tire forces are treated as random walk signal, which implies that it does not involve dynamic equation at all.

The measurement noise error covariance matrix was chosen as $\mathbf{R}$ = diag[0.0001, 0.001, 0.0001, 0.0001, 0.000001, 0.01, 0.01, 0.01, 0.01] based upon the actual test data and equipment specifications. And the process noise error covariance matrix was chosen as $\mathbf{Q}$ = diag[1, 1, 0.0001, 0.01, 0.01, 0.01, 0.01, 1, 1, 1, 1, 1000, 1000, 1000, 1000].

State vector can be estimated by applying discrete-time EKBF as follows (Ray, 1997; Simon, 2006):

$$\begin{aligned} \hat{\mathbf{x}}_k^- &= \hat{\mathbf{x}}_{k-1}^+ + \int_{t_{k-1}}^{t_k} f\left(\hat{\mathbf{x}}(\tau), \mathbf{u}(\tau)\right) d\tau \\ \mathbf{P}_k^- &= \mathbf{P}_{k-1}^+ + \int_{t_{k-1}}^{t_k} \left\{\mathbf{F}(\tau)\mathbf{P}(\tau)+\mathbf{P}(\tau)\mathbf{F}^{\mathrm{T}}(\tau)+\mathbf{Q}(\tau)\right\} d\tau \\ \mathbf{K}_k &= \mathbf{P}_k^-\mathbf{H}_k^{\mathrm{T}}\left[\mathbf{H}_k\mathbf{P}_k^-\mathbf{H}_k^{\mathrm{T}}+\mathbf{R}\right]^{-1} \\ \hat{\mathbf{x}}_k^+ &= \hat{\mathbf{x}}_k^- + \mathbf{K}_k[\mathbf{z}_k - \mathbf{H}_k(\hat{\mathbf{x}}_k^-)] \\ \mathbf{P}_k^+ &= \left[\mathbf{I}-\mathbf{K}_k\mathbf{H}_k\right]\mathbf{P}_k^- \end{aligned} \tag{30}$$

Here, $\mathbf{F}$ and $\mathbf{H}$ are Jacobian matrices of process and measurement model, respectively,

$$\mathbf{F} = \frac{\partial f(\hat{\mathbf{x}}_k^-, \mathbf{u}_k)}{\partial \hat{\mathbf{x}}_k^-},\ \mathbf{H}_k = \frac{\partial h(\hat{\mathbf{x}}_k^-, \mathbf{u}_k)}{\partial \hat{\mathbf{x}}_k^-} \tag{31}$$

Computation of the discrete-time EKBF gain is a subtle mix of processing and measurement noise. Since the measurements have high accuracy, $\mathbf{R}$ matrix was set with small values in this task.

5. EXPERIMENTAL RESULTS

5.1. Experimental Setup

This section presents the experimental studies carried out to obtain the real tire forces. The equipment and proving

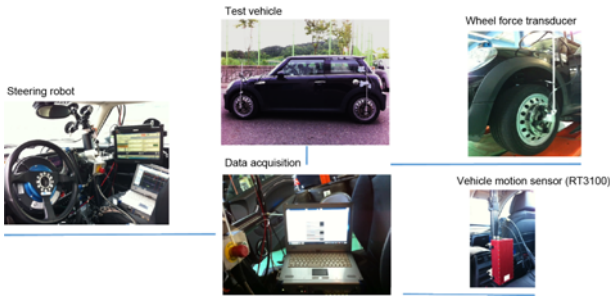

Figure 3. Implementation of data acquisition devices for the estimator validation.

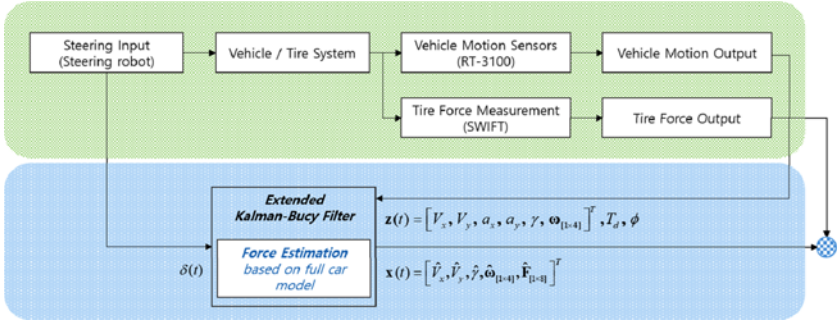

Figure 4. Block diagram of estimator and validation process.

ground were provided by Hankook tire R&D center. The test vehicle is a B class hatchback with 195/55R16 size summer tires.

To input an accurate hand-wheel steering angle, steering robot was equipped with the vehicle. Vehicle motion was recorded by RT-3100® IMU/GPS sensor and tire forces was measured by SWIFT®. All the data was collected at 100 Hz sampling frequency. The implementation of the stearing input and acquisition devices is illustrated in Figure 3.

Figure 4 shows the block diagram of the estimator and validation process. From the vehicle motion sensors, measurement vector $\mathbf{z}(t)$ that is used for posteriori estimation of EKBF was obtained. In addition, vehicle drive torque was calculated from the vehicle motion sensor values, which was explained in Section 2.3.

To validate the estimation performance that includes considerable weight shifting of the vehicle, an open loop test with a highly severe maneuvering mode was conducted. A triangular shape $+40^{\circ} \rightarrow -100^{\circ} \rightarrow +60^{\circ}$ hand-wheel steering angle input during a 1.2 second time period was adopted for a reference scenario (see Figure 5 (a)). This mode was severe enough to cause the nonlinear behaviour of the vehicle lateral motion. And the test was conducted

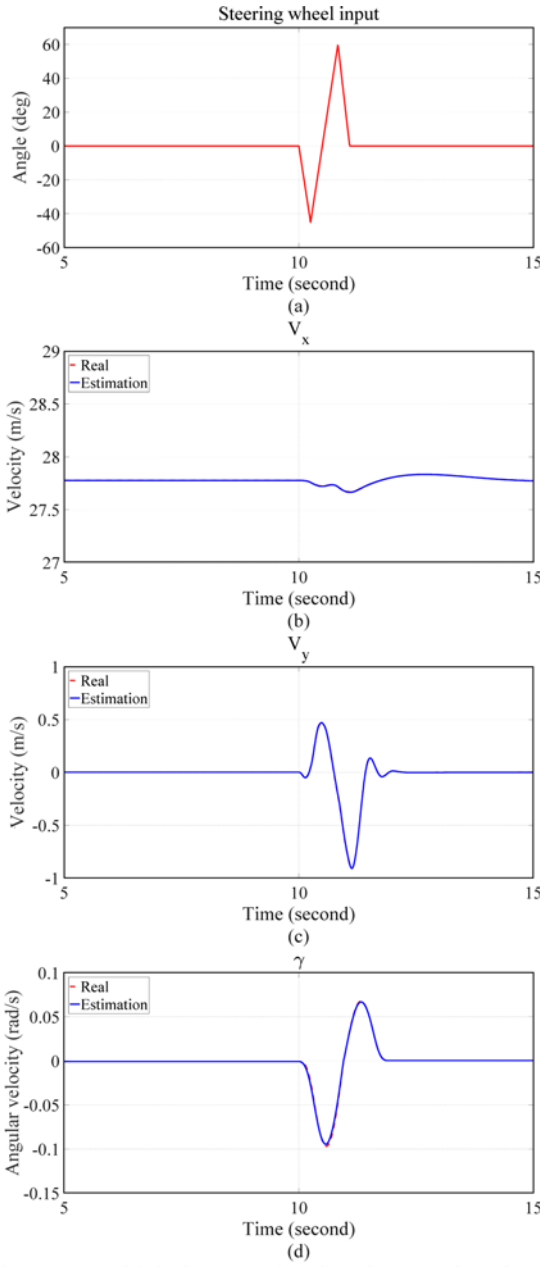

Figure 5. Vehicle input and estimation results of vehicle motion states: (a) Steering wheel angle; (b) Longitudinal velocity; (c) Lateral velocity; (d) Yaw rate.

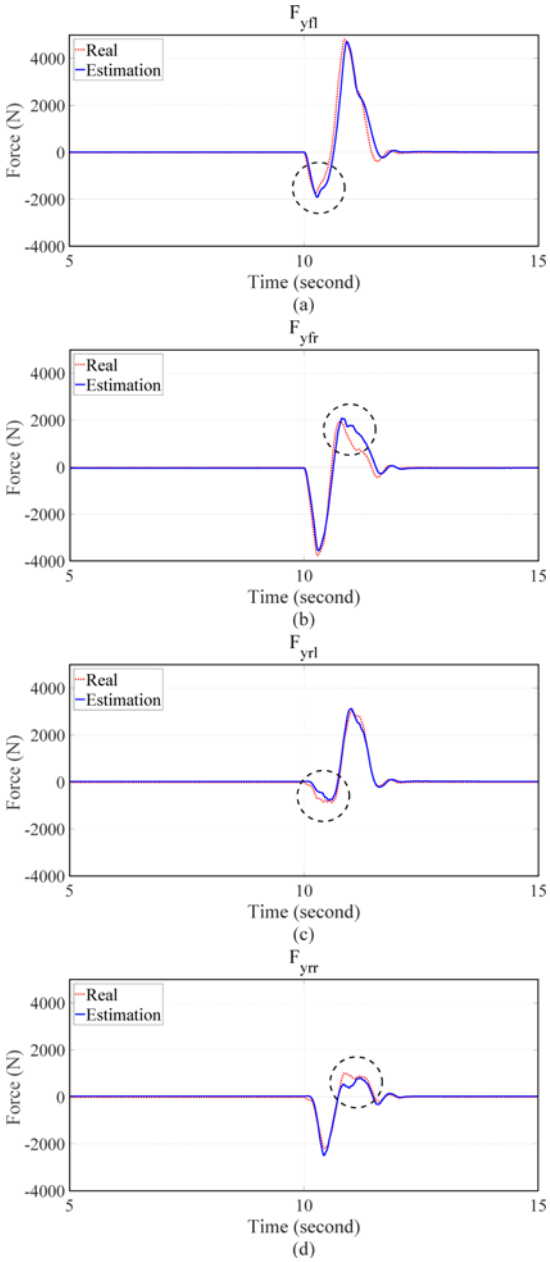

Figure 6. Estimation results of lateral tire forces: (a) Front left; (b) Front right; (c) Rear left; (d) Rear right.

by an expert driver to maintain constant longitudinal speed.

5.2. Vehicle Motion Validation

At first, estimated vehicle states were compared with the experimental data. Figure 5 represents the estimation results of the longitudinal velocity, lateral velocity and yaw rate for the reference steering input. Although the test was conducted at a highly severe mode, the results reveal very accurate estimation performance. The root mean square (RMS) errors of estimated motion states are 0.227 m/s, 0.0018 m/s and 0.000613 rad/s.

5.3. Lateral Tire Force Validation

$\hat{\mathbf{F}}_y(t) = [\hat{F}_{yfl}, \hat{F}_{yfr}, \hat{F}_{yrl}, \hat{F}_{yrr}]^T$ was obtained from the tire force estimator, and then it was compared with the experimental data. Figure 6 shows the estimation results of the lateral tire force at all wheel positions. The RMS estimation errors of each tire are 234 N, 201 N, 193 N and 161 N on front left tire, front right tire, rear left tire and rear right tire respectively. Considering the bigger maximum lateral tire force of front wheel than that of rear one, it is reasonable that the RMS error of the estimation accuracy of tire force at front wheel is larger than the rear one. Experimental results prove that the suggested estimator is sufficiently functional in the test with a maximum lateral force over 4000 N. However, the performance of the observer was deteriorated over inner wheels at which tire grip force is not generated much due to the less vertical load than outer wheels (see black dotted circles of Figure 6). More specifically, estimation error was worse at rear wheels than that of front wheels during the counter steer motion. This was mainly due to the absence of suspension and vehicle torsional stiffness models. Without those models, the difference of the weight shifting effects between the front and rear axles cannot be described accurately.

6. CONCLUSION

In this paper, estimation method of the tire forces at all wheel positions was suggested. The eleven degree of freedom vehicle model was designed with the planar full car model and the reference tire model. In particular, the modified tire relaxation length was applied to the lateral tire dynamic model and the cornering stiffness that includes the weight shifting effect was applied to the lateral steady tire model in order to improve estimation accuracy of the lateral tire forces for severe transient maneuvers. Then, the discrete-time EKBF estimation strategy was applied to estimate the states of vehicle motions and tire forces, which have nonlinear characteristics. The performance of the suggested estimator were validated by the comparison with the experimental data. The experimental results showed very accurate estimation performance even under the extremely transient test mode of double lane change. The suggested estimator is expected to assist vehicle and tire design engineers in estimating the tire force more accurately. With the accurate tire force information, performance of vehicle chassis control systems can be improved greatly. Moreover, the estimated tire forces can be applied to the derivation of empirical tire model that can supplement the indoor test results.

ACKNOWLEDGEMENT−The authors would like to appreciate Hankook tire Co. Ltd. for provision of experimental equipment and devices. This research was supported by the MSIP (Ministry of Science, ICT and Future Planning), Korea, under the ITRC (Information Technology Research Center) support program (IITP-2017-2012-0-00628) supervised by the IITP (Institute for Information & communications Technology Promotion). This work was supported by the National Research Foundation of Korea (NRF) grant funded by the Korea government (MSIP) (No. 2017R1A2B4004116).

REFERENCES

Baffet, G., Charara, A. and Dherbomez, G. (2007). An observer of tire-road forces and friction for active security vehicle systems. *IEEE/ASME Trans. Mechatronics* **12**, **6**, 651−661.

Doumiati, M., Victorino, A. C., Charara, A. and Lechner, D. (2011). Onboard real-time estimation of vehicle lateral tire – Road forces and sideslip angle. *IEEE/ASME Trans. Mechatronics* **16**, **4**, 601−614.

Dugoff, H., Fancher, P. S. and Segel, L. (1970). An analysis of tire traction properties and their influence on vehicle dynamic performance. *SAE Paper No*. 700377.

Gillespie, T. D. (1992). *Fundamentals of Vehicle Dynamics*. SAE International. Warrendale, Pennsylvania, USA.

Han, K., Hwang, Y., Lee, E. and Choi, S. (2016). Robust estimation of maximum tire-road friction coefficient considering road surface irregularity. *Int. J. Automotive Technology* **17**, **3**, 415−425.

Heydinger, G. J., Garrott, W. R. and Chrstos, J. P. (1991). The importance of tire lag on simulated transient vehicle response. *SAE Paper No*. 910235.

Higuchi, A. and Pacejka, H. (1997). Tire relaxation length concept at large wheel slip and camber. *Vehicle System Dynamics: Int. J. Vehicle Mechanics and Mobility* **27**, **1**, 50−64.

Kim, J. (2009). Nonlinear tire force estimation and road friction identification: Simulation and experiments. *Control Engineering Practice* **17**, **3**, 357−367.

Lee, E., Lee, J. and Choi, S. (2016). String tire model for evaluating steering agility performance using tire cornering force and lateral static characteristics. *Vehicle System Dynamics: Int. J. Vehicle Mechanics and Mobility* **55**, **2**, 231−243.

Maas, J. W. L. H. (2009). *A Comparison of Dynamic Tyre Models for Vehicle Shimmy Stability Analysis.* M. S. Thesis. Eindhoven University of Technology. Eindhoven, Netherlands.

Pacejka, H. (2005). *Tire and Vehicle Dynamics.* Elsevier. Oxford, UK.

Ray, L. R. (1997). Nonlinear tire force estimation and road friction identification: Simulation and experiments. *Automatica* **33**, **10**, 1819−1833.

Schilippe, B. V. (1954). Shimmying of a Pneumatic Wheel (English Translation Ver. of Das Flattern Eines Bepneuten Rades). NACA TM 1365, 125−147.

Simon, D. (2006). *Optimal State Estimation: Kalman, H Infinity, and Nonlinear Approaches*. John Wiley & Sons. New Jersey, USA.

APPENDIX

Table A.1. Modelling parameters of the test vehicle body and tire.

Parameter	Value
Distance from CG to front and rear axle, l_f, l_r	1.25 m, 1.217 m
Height from ground to CG, h_{cg}	0.4 m
Distance from the CG to the roll axis, h_r	0.15 m
Front and rear track width, t_f, t_r	1.461 m, 1.461 m
Effective wheel radius, R_e	0.3 m
Vehicle curb weight + 1 driver + test equipment, m	1250 kg
Vehicle moment of inertia about yaw axis, I_z	3350 kg m^2
Wheel moment of inertia, I_w	0.6 kg m^2
Front and rear roll steer coefficient, ε_f, ε_r	0.07, 0.08
Front and rear roll stiffness, $c_{\varphi f}$, $c_{\varphi r}$	650 Nm/rad, 650 Nm/rad
Cornering stiffness relation coefficients, c_1, c_2	21, 18.1
Lateral stiffness, K_L	128422 N/m
Distortion stiffness, K_D	5080 Nm/rad
Adjustment factors, k_1, k_2	0.98, 0.99